Journal of Materials Processing Technology 212 (2012) 1591–1597

Contents lists available at SciVerse ScienceDirect

Journal of Materials Processing Technology

journal homepage: www.elsevier.com/locate/jmatprotec

Metal injection moulding of CP-Ti components for biomedical applications

A.T. Sidambe[a,*], I.A. Figueroa[a,1], H.G.C. Hamilton[b], I. Todd[a]

[a] University of Sheffield, Materials Science and Engineering Department, Sir Robert Hadfield Building, Mappin Street, Sheffield S1 3JD, UK
[b] Johnson Matthey Technology Centre, Blount's Court, Sonning Common, Reading, Berkshire RG4 9NH, UK

ARTICLE INFO

Article history:
Received 19 April 2011
Received in revised form 28 January 2012
Accepted 2 March 2012
Available online 10 March 2012

Keywords:
Metal injection moulding
Titanium
Titanium alloys
CP-Ti
Debinding
Sintering
Solvent debinding
Solid polymer solution
Thermal debinding

ABSTRACT

Titanium exhibits properties that are excellent for various applications but the processing routes remain expensive and difficult. Metal injection moulding is a processing route that offers reduction in costs, with the added advantage of near net-shape components. In this study, the commercially pure (CP-Ti) powder was subjected to metal injection moulding studies in order to investigate its suitability for biomedical applications. The CP-Ti with powder size of sub 45 μm was mixed with a binder which consists of a water soluble component, injection moulded and then sintered. The mechanical and impurity level properties of the final components were then determined and found to be within ASTM Grade 2 (ASTM F67) specifications for titanium. The debinding mechanisms, kinetics and chemical reactions are analysed and discussed in detail in this study.

1. Introduction

Titanium and titanium alloys exhibit a high specific strength and stiffness, outstanding corrosion resistance and biocompatibility. This combination of properties makes titanium and its alloys an excellent choice for applications in watch parts, dental parts and sports goods as was reported by Shibo et al. (2006), and also provides a great potential for biomedical and aerospace applications. In biomedical applications, commercially pure titanium was reported by McCracken (1999) and Elias et al. (2008) to be used preferentially for endosseous dental implant applications. However, the processing of titanium is limited by costly, multi-step process of fabrication and associated geometry design constraints as reported by Ferri et al. (2009). Ebel et al. (2011) recently reiterated that metal injection moulding (MIM) is a technique that can provide minimisation of such problems and may contribute to the development of Ti implants with higher functionality without increasing the price.

MIM is a well-established, cost-effective method of fabricating small-to-moderate size metal components. In this process metallic powders are injected into a mould. Plasticity and fluidity of the powder is essential for this to take place and this is achieved by the use of binder material. All binder systems are based on two important major groups of ingredients, polymers and waxes with minor additions of lubricants, surfactants and coupling agents. After injection moulding, the binders are then removed in a process known as debinding and the remaining "brown" part is then sintered at elevated temperatures to achieve a densified part.

In the metal injection moulding of titanium, there have been serious challenges in recent years. Froes (2005), German (2009), German (2010) and Ebel et al. (2011) singled out the oxygen and carbon levels in the sintered parts as having been too high for structural use, which meant that the titanium produced could not conform to standards required for biomedical applications such as implants.

Much of the early work on developing a viable titanium MIM process was plagued by the unavailability of suitable powder, less than optimum binders and debinding processes for a material as reactive as titanium, and inadequate protection of the titanium during elevated temperature processing. Petzoldt et al. (1995), Froes and German (2000) and Shibo et al. (2009) discussed various measures that have been taken to improve the properties of titanium parts produced via MIM, including careful binder selection. Several other binder formulations have recently been reported by Baril et al. (2011) as having been developed for MIM of titanium. The formulations which generally include polyethylene, polypropylene, polymethylmethacrylate, polyethylene glycol, ethylene vinyl

* Corresponding author. Tel.: +44 (0)114 222 6035; fax: +44 0114 222 5943.
E-mail address: A.T.Sidambe@sheffield.ac.uk (A.T. Sidambe).
[1] Permanent address: Instituto de Investigaciones en Materiales, UNAM, 04510 México, D. F., México.

0924-0136/$ – see front matter © 2012 Elsevier B.V. All rights reserved.
doi:10.1016/j.jmatprotec.2012.03.001

Table 1
CP-Ti chemical properties.

Powder type	Size (μm)	Composition (%)					
		O	C	N	H	Fe	Ti
CP-Ti	Sub 45	0.143	0.012	<0.05	<0.05	0.06	Bal.

acetate, paraffin wax, naphthalene and stearic acid have been used to produce titanium via MIM as reported in reviews by Froes (2007), German (2009) and Park et al. (2009).

During debinding, the decomposition mechanisms and chemical composition of binder play a major role in levels of residual contamination. Therefore in order to reduce contamination of Ti with carbon and oxygen due to debinding, the requirement is to reduce the amount of decomposable substances in the binder. At the same time the binder has to provide enough residual strength so that the component can be handled after debinding as stated by Shibo et al. (2009).

One of the standards that have been used in the past to characterise Ti MIM is the ASTM F67 from the American Society for Testing Materials (ASTM Standard F67-06 2006) and its specifications cover the chemical, mechanical, and metallurgical requirements for four grades of unalloyed titanium strips, sheets, plates, bars, billets, forgings, and wires used for the manufacture of surgical implants. However, at the time of writing up this publication, a proposed new standard for four different grades of metal injection moulded CP-Ti components to be used in the manufacture of surgical implants has been placed under development by ASTM (ASTM Standard WK35394, 2011). For alloyed Ti6Al4V, equivalent standards have already been released (ASTM Standard F2885-11, 2011).

This study therefore describes the MIM process which employs a binder with a water soluble component and with reduced decomposing substances. The binder system, which uses water soluble PEG, was first reported by Cao et al. (1992) after they developed a binder made of a major fraction of polyethylene glycol (PEG) and a minor fraction of PMMA polymer. Other uses of PEG as the primary water-soluble component have been reported by Hens and German (1993) where the PEG aided in designing feedstock systems aimed at maximising the ease of processing and shape retention during debinding and sintering, while minimising processing times.

The PEG based water soluble binder system has since been used widely with other ceramic and metallic powders, including titanium and its alloys. Yang et al. (2003) studied the solvent debinding mechanism for alumina injection moulded compacts whilst Anwar (1996), Omar et al. (2006) and Eroglu and Bakan (2005) used 316L stainless steel powder as a test material. However, one report by Einhorn et al. (1997) discouraged the use of binder with a water soluble component in the MIM of Ti on the basis that such binders give increased oxygen content in the parts which in turn affect the mechanical properties and hence the suitability for biomedical applications.

In this study a binder consisting of polyethylene glycol (PEG), polymethylmethacrylate (PMMA) and stearic acid (SA) is investigated for its ability to produce titanium components that can be used in biomedical applications. The debinding chemical reactions and the debinding mechanisms are discussed in detail.

2. Experimental

The CP-Ti powder used in this study was supplied by Advanced Powders and Coatings (Raymor Inc., Canada) and is produced by plasma atomisation. Table 1 shows the CP-Ti chemical properties that were obtained via X-ray fluorescence (XRF). Fig. 1 is a scanning electron micrograph (SEM) showing the morphology of the powder as spherical in shape. All the characterisations carried out via SEM

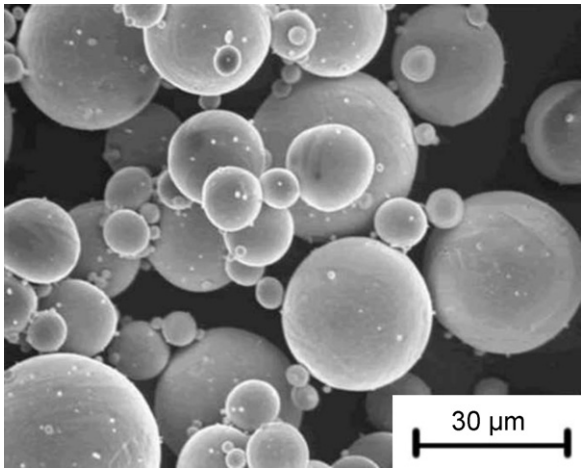

Fig. 1. Scanning electron micrograph showing the morphology of the CP-Ti.

were done on the Camscan Mk II (Cambridge Scanning, UK). The particle size distribution is shown in Fig. 2 as sub 45 μm in size and this was obtained using a Coultier LS particle size analyser with sonication and diffloculant used to break up agglomerates.

The CP-Ti powder was mixed with a binder that consists of a major fraction of water soluble polyethylene glycol with molecular weight of 1500 (PEG_{1500}) and a minor fraction of polymethylmethacrylate with a molecular weight of 10^6 ($PMMA^6_{10}$) with stearic acid (SA) used as a surfactant.

The PEG was supplied by Sigma–Aldrich and at the molecular weight of 1500 g/mol, the PEG is in a crystalline form. PEG has in the crystalline state has a fairly open helical structure and this structure is responsible for the low melting temperature of 45–50 °C and its solubility in water as reported (Elias, 2003). The PMMA was supplied by Scott Bader Co. Ltd (Wellingborough, UK). The chemical structures of the PEG and the PMMA are shown in Fig. 3. The simplest degradation of PMMA occurs at very high molecular weights as explained (Hsu, 1999).

Handling of the materials was carried out in an inert argon atmosphere and the mixing was carried out in the centrifugal Speedmixer™ 800 FZ (Hauschild; supplied by Synergy Devices Ltd, UK). The mixing speeds were increased every 2 min as follows:

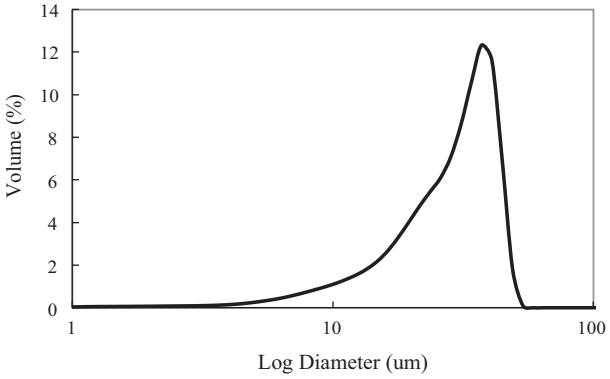

Fig. 2. Particle size distribution for CP-Ti.

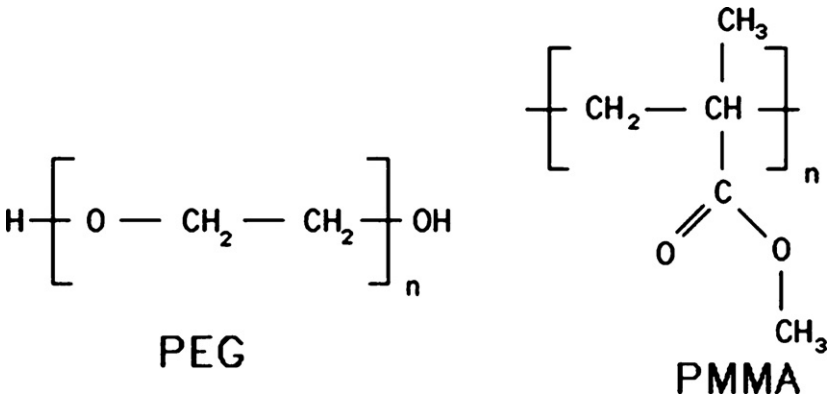

Fig. 3. Chemical structures of PEG and PMMA.

800, 1200, 1400, 1400, 1600 rpm, leading to a total mixing time of 10 min. The weight ratios of the constituent binder materials were 87:11:2 of PEG, PMMA and SA respectively. A critical powder loading of 69 vol% was obtained via rheological studies carried out on a Rosand RH2000 capillary rheometer (Malvern Instruments, UK).

The mixed feedstock was granulated and then injection moulded in a 60 t Arburg 320 C (Arburg, Germany) injection moulding machine at 120 °C. An injection pressure of 1500 bar, packing pressure of 1350 bar and injection speed of 30 cm^3/s were used. An MPIF Standards 35 mould was used to mould tensile bars and after injection moulding, the mouldings were visually inspected and each weighed for quality control.

The green part mouldings were subjected to solvent extraction by immersing them in a heated water bath containing distilled water for 6 h at 55 °C. This stage of debinding was aimed at removing the PEG component of the binder. The MIM samples were then dried in air at 40 °C for 12 h.

The parts were then subjected to thermal debinding in order to remove the backbone PMMA binder in a Centorr VI MIM-Vac M200 Series 3570 furnace (Nashau, USA). This was done by heating the parts in an argon atmosphere at a ramp rate of 2.5 °C/min to 350 °C, and holding for 1 h after which they were heated up again at a heating rate of 2 °C/min to 440 °C and again holding for 1 h.

Sintering was carried out in the furnace during the same cycle with the thermal debinding. The sintering carried out under the control of four sintering factors; sintering time, sintering atmosphere, heating rate and the sintering temperature. The conditions that were selected for the sintering of the CP-Ti parts are; sintering time of 3 h, sintering in argon with a retort flow rate of 10 slpm, heating rate of 10 °C/min and sintering temperature of 1300 °C. During thermal debinding and sintering, the partial pressure in the furnace was set at 300 Torr (~400 mbar). The results of the study which was carried en route to obtaining the optimum processing parameters of solvent and thermal debinding used here have been published by Sidambe et al. (2008). The optimisation of the sintering process was carried out using the Taguchi L9 experimental method and the details of this study have also been published by Sidambe et al. (2009, 2011a,b). However, in these two publications the extents to which the debinding mechanisms, kinetics and chemical reactions affect the final sintered component were not discussed in detail. In this study, the focus is on the debinding route.

Differential scanning calorimetry (DSC) studies in order to observe phase transitions were carried out on a Perkin Elmer DSC machine (MA, USA). Tests to determine changes in weight loss in relation to change in temperature and PMMA decomposition were carried out also using a Perkin Elmer TGA machine. The chemical analysis of the sintered samples to determine the impurity levels of oxygen and carbon of MIM specimens was carried out using a conventional LECO melt extraction system by London & Scandinavian Metallurgical Laboratories (Rotherham, UK). Mechanical tests were carried out at room temperature according to ASTM E8 standards by NDT Ltd (Sheffield, UK).

3. Results

3.1. Rheology and feedstock

Fig. 4 shows the evolution of the viscosity with temperature of the 69 vol% CP-Ti feedstock mixed with PEG, PMMA and SA at weight ratios of 87:11:2 respectively.

It can be seen from the shear viscosity vs shear rate plot that the flow is pseudo plastic with the viscosity decreasing with increasing shear rate, the viscosity being lower at the higher temperature of 120 °C and increasing with lower temperature. It is desirable that the viscosity of the feedstock should decrease quickly with increasing shear rate during injection with no dilatants behaviour. This was the case with the CP-Ti feedstock and rheology indicates improved homogeneity of feedstock. This is confirmed in Fig. 5 which is a scanning electron micrograph of a moulding fracture surface which shows the distribution of the CP-Ti powder within the PEG/PMMA/SA binder system. The binder, as can be seen, is evenly distributed throughout the sample body.

3.2. Solvent debinding

Fig. 6 shows two scanning electron micrographs which illustrate the typical development of pores during the removal of PEG in heated distilled water. After an hour of solvent debinding, it can be seen that there is still some residual PEG within the Ti/PMMA matrix. After 4 h of solvent debinding, the SEM shows virtually no PEG with the remaining strands of binder consisting of PMMA.

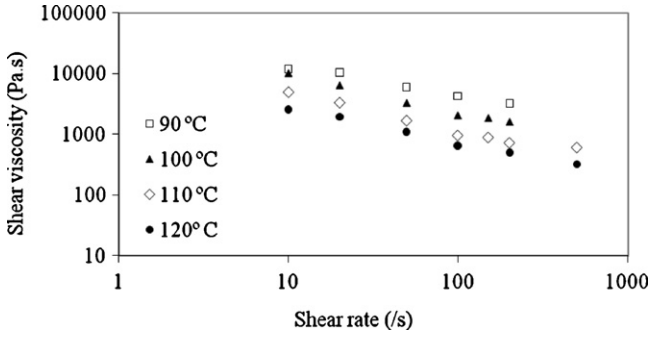

Fig. 4. Apparent viscosity vs apparent shear rate of 69 vol% Ti feedstock at different temperatures.

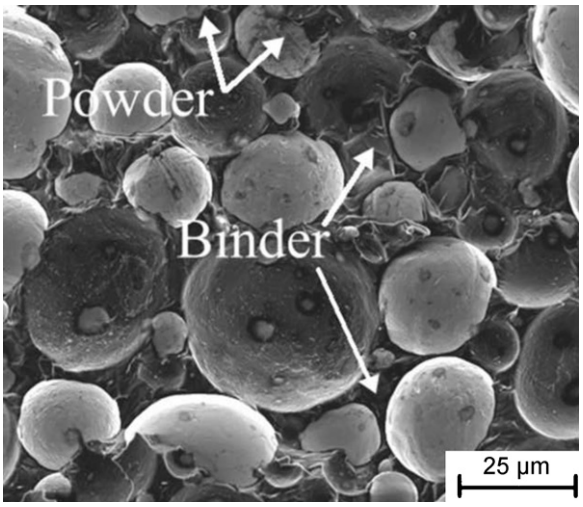

Fig. 5. Scanning electron micrograph of an as moulded component surface.

The complete removal of PEG was achieved at 55 °C after 5 h with no defects such as cracks. Fig. 7 shows the amount of PEG that was removed by water leaching from mouldings plotted against the leaching time at 55 °C.

Fig. 8 is a graph taken from a DSC and shows scans of a selected as moulded CP-Ti green specimen and that of a typical leached part after solvent debinding. The graph shows the absence of the PEG component in the leached samples as there is no peak corresponding to the heat flow as a result of PEG. The DSC also shows the peak for the PEG at 44 °C indicating the melting temperature.

3.3. Thermal debinding

Fig. 9 is a scanning electron micrograph which shows a typical brown part after the removal of the PMMA during thermal pyrolysis. The PMMA strands that were remaining behind as shown in Fig. 6 have been eliminated, indicating successful debinding. The results can even be verified further by TGA analysis.

Fig. 10 is a TGA trace showing weight loss of CP-Ti/Binder mix before and after thermal pyrolysis. It can be seen that there is no recorded weight loss from the brown part after thermal pyrolysis which confirms the complete removal of the PMMA binder component. Fig. 10 also shows the decomposition characteristics of the PMMA which degrades at 200–430 °C. This information is useful in setting the thermal debinding process parameters. Binder unzipping under argon occurs over a shorter period than in air.

3.4. Sintering

The CP-Ti feedstock used here contains a relatively high volume of binder at 31%. Therefore after the complete removal of the binder and subsequently the sintering, the linear shrinkage was found to be 11 ± 1%. Fig. 11 is a photograph illustrating the linear shrinkage undergone by a sintered CP-Ti MIM tensile sample. The dimensional change of the MIM sample after injection moulding and sintering is shown with good shape retention.

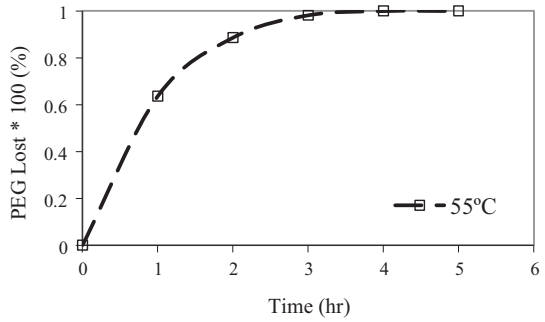

Fig. 7. Amount of PEG removed from the moulding vs the leaching time at 55 °C.

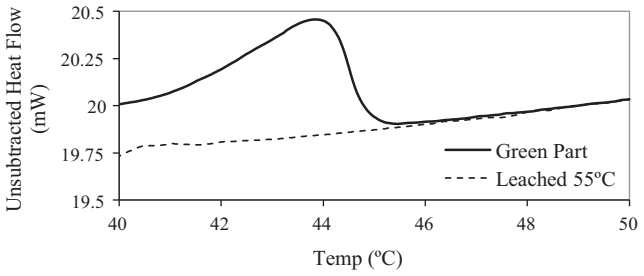

Fig. 8. DSC showing scans of an as moulded CP-Ti green specimen and that of a leached part after solvent debinding. The scans were carried out at 2 °C/min.

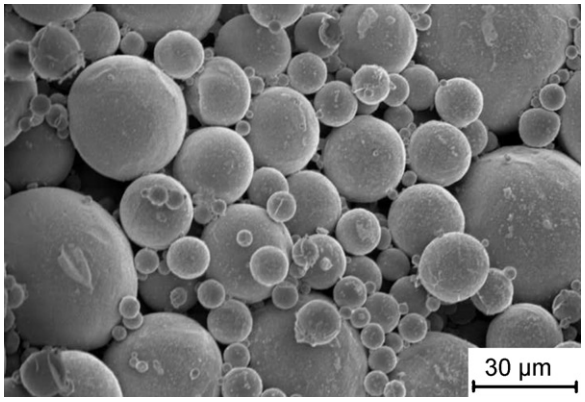

Fig. 9. Scanning electron micrograph which shows the brown part after the removal of the PMMA during thermal pyrolysis.

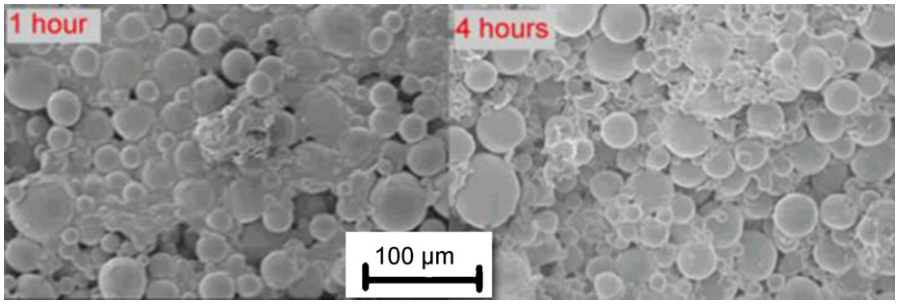

Fig. 6. Scanning electron micrographs showing the development of pores during the removal of PEG.

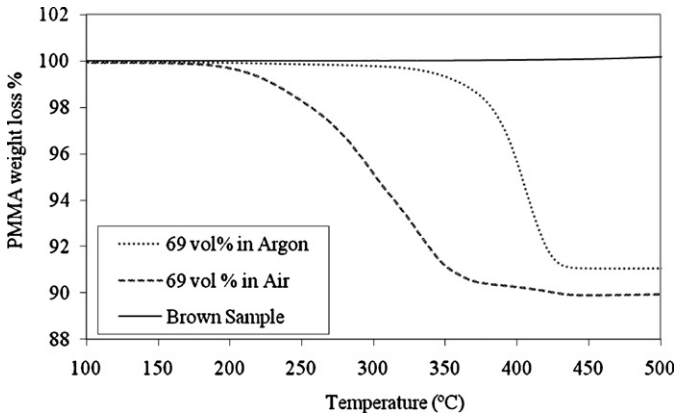

Fig. 10. Weight loss curves for PMMA at a heating rate of 5 °C/min for Ti/binder mix in argon and in air before and after thermal pyrolysis.

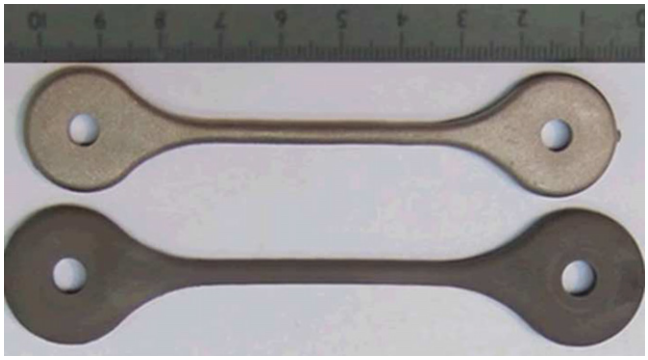

Fig. 11. Photograph illustrating the linear shrinkage undergone by a MIM sintered CP-Ti part.

The final mechanical and chemical properties of selected CP-Ti injection moulded standard tensile bars are shown in Table 2. From Table 2 it can be seen that CP-Ti properties for oxygen impurity levels and elongation are that of Grade 2 according to ASTM F67-06 specifications. The tensile strength is above Grade 1 requirements. The residual carbon level was 0.04% in one of the sintered Ti sample analysed. The maximum requirement for carbon is 0.08%.

Table 2
CP-Ti injection moulded component mechanical and chemical results.

Sample	Tensile strength (MPa)	Elongation (%)	Oxygen (%)	Porosity (%)
1	483	21	0.21	3.5
2	460	24	0.21	4.2
3	467	21.5	0.19	3.0
4	475	20	0.20	5.2
5	466	27	0.19	4.7
6	451	24.5	0.17	3.8

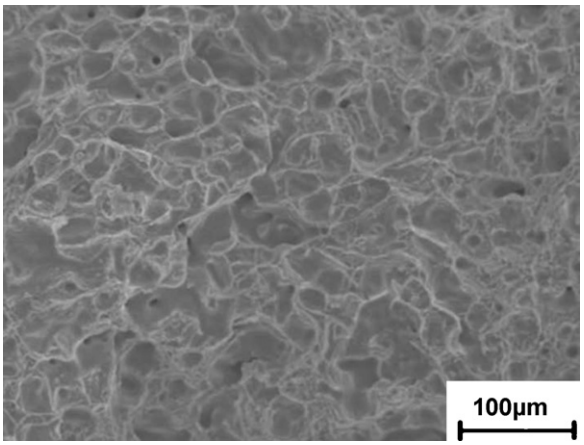

Fig. 13. Fracture surface of a CP-Ti MIM-tensile test sample after mechanical test showing honeycomb structure which signifies a typical sign for a ductile break.

The porosity of the samples that was measured using image analysis ranges from 3% to 5.2%. ASTM Standard F2885 for Ti64 MIM specifies that the porosity should not exceed 4%.

Shown in Fig. 12 is the pore structure and microstructure of the six selected CP-Ti MIM components which indicates a low void ratio of round unconnected pores. Fig. 13 is an SEM of the typical fracture surface of a CP-Ti MIM-tensile test sample after mechanical test showing honeycomb structure which signifies a typical sign for a ductile break.

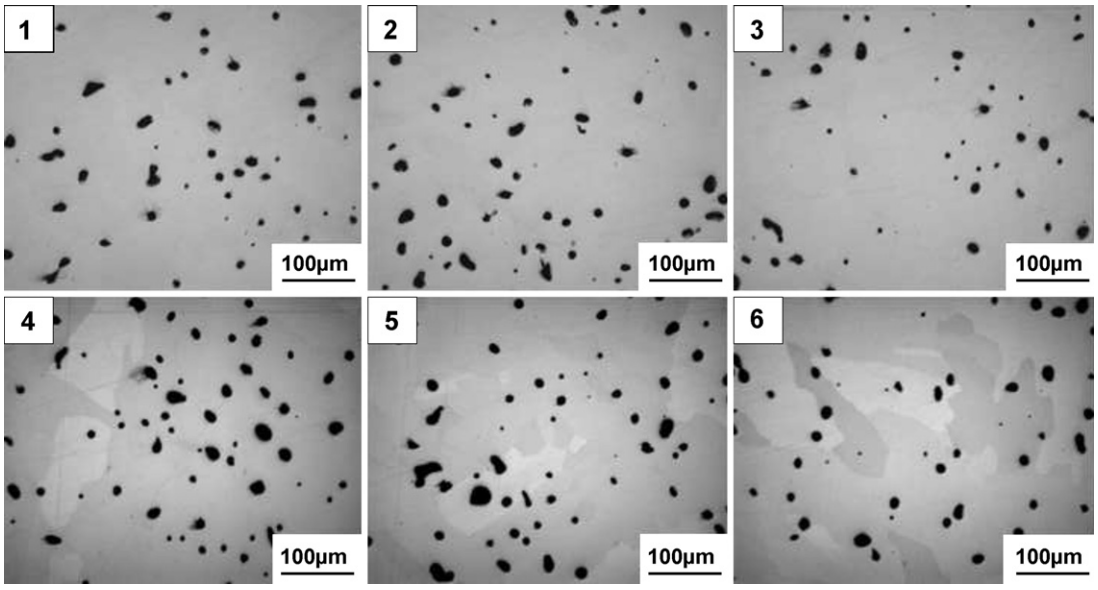

Fig. 12. The pore structure of the sintered CP-Ti MIM compacts.

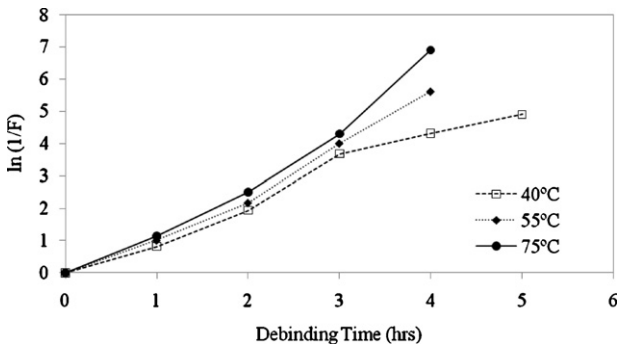

Fig. 14. ln(1/*F*) with leaching time at 40, 55 and 75 °C. *F* is the remaining fraction of PEG.

4. Discussion

Because it is crucial in MIM components for biomedical implants that there is no residual binder left behind in the final part, it is important to discuss in detail the mechanisms through which this has been achieved in this study.

4.1. Solvent debinding

Commercially pure titanium (CP-Ti) is considered to be the best biocompatible metallic material because its surface properties result in the spontaneous build-up of a stable and inert oxide layer as reported (Elias et al., 2008). The first debinding process, i.e. solvent debinding, does not involve polymer decomposition. The chemical analysis results shown in Table 2 confirm that leaching CP-Ti MIM samples in water does not increase oxygen levels detrimentally. Titanium metal contains a surface layer of titanium oxide that prevents chemical reactions. When the layer is damaged it is usually restored rapidly. Titanium only reacts with water after its protective titanium oxide surface layer is destroyed. It is therefore water insoluble.

Pertaining to kinetics, solvent debinding is a two-stage process consisting of dissolution and diffusion. Initially, the solvent dissolves the polymer phase, thus forming porous surface. The solvent then gets into the pores by capillary action. This is followed by diffusion of dissolved polymeric substances out of the green body. The process can be formulated using Fick's diffusion-based model that has been reported by Kim et al. (2007):

$$\ln\left(\frac{1}{F}\right) = \frac{D_e t \pi^2}{(2L)^2} + K \tag{1}$$

where F is the fraction of the remaining soluble polymer, D_e is the inter-diffusion coefficient of polymer and solvent, t is time, $2L$ is the thickness of the specimen and K represents the change in the mechanism controlling the debinding behaviour.

Eq. (1) can be utilised to explain solvent debinding behaviour of PEG for the injection moulded CP-Ti powder. In order to demonstrate that solvent debinding is a two stage process, results have been included in Fig. 14 for the debinding temperatures of 40 and 75 °C where ln(1/*F*) is plotted against leaching time. At 40 °C it is clear that the solvent debinding is a two-stage process. The dissolution of PEG is the rate limiting step in the beginning of debinding up to leaching time of 3 h. As the process proceeds, a longer diffusion distance through porous channels formed after initial debinding slows down the process and diffusion becomes rate-determining step.

4.2. Thermal pyrolysis

The backbone PMMA is removed by decomposition. The decomposition was explained by Jellinek (1978) who stated that the PMMA retro polymerises into monomers with the production of gaseous product but leaves no residue and that the range of monomer (MMA) yielded in the process is from 95% to 100% in vacuum or inert atmospheres. The residual oxygen and carbon levels obtained in the sintered samples suggest that the titanium surfaces do not interact significantly with PMMA or its degradation products. During the process, several mass transport processes often occur simultaneously during binder removal but in the case of the Ti/PMMA body it is the pore structure of the partially debound body which influences the resistance to mass transfer. The pre-existing porosity allows for fast vapour transport, making the body relatively easy to debind.

Apart from the pore structure, the carefully controlled heating rate and the partial pressure in the furnace, on which the mean free path depends, are designed to control the capillary forces and limit defect formation. At the set partial pressure of 300 Torr or 400 mbar, the velocity of the inert (argon) gas molecules is sufficient to allow for smooth and even flow over surface irregularities. According to Joens (2005), this creates an even flow and no shadow effects, much as if the parts were submerged in a liquid. At an atmospheric pressure of 760 Torr, the gas molecules would flow at high pressure and velocity, colliding with each other whereas at a molecular flow of 1 Torr or less, the gas molecules are known to collide with each other randomly and gas flow becomes unpredictable.

The transport of gaseous species through empty pores occurs by either Knudsen slip, or viscous (Poiseuille) flow as demonstrated by German (1979). The flow mechanism was also used by Tsai (1991) when they analysed pressure build up and internal stresses during binder burnout and by Song et al. (1996) in modelling the effect of gas transport during thermal debinding. The Knudsen flow which was originally formulated by Knudsen (1909) occurs when the average pore radius (r) is much smaller than the mean free path (λ_g), i.e. $r/\lambda_g < 0.1$. Slip flow occurs when gas transport is intermediate between viscous flow and Knudsen flow, i.e. r/λ_g is in the range of 0.1–10 and, finally, viscous flow occurs when $r/\lambda_g > 10$ as was demonstrated (Lewis, 1997).

The process of gas transport through the pores can be estimated using an expression developed by Wakao et al. (1965) to estimate K, the transport coefficient for a single gas through a capillary of radius r:

$$K = \frac{1}{RT}\left[\frac{(2r/3)\sqrt{8RT/\pi M_W}}{1+2r/\lambda} + \frac{1}{1+\lambda(2r)}\left(\frac{\pi r}{6}\sqrt{\frac{8RT}{\pi M_W}} + \frac{r^2 p}{8\eta}\right)\right] \tag{2}$$

where R is the gas constant, T is temperature, M_w is molecular weight of the gaseous species, P is pressure, and η is the viscosity of the gas given by:

$$\eta = \frac{M_W \bar{\nu}}{3\sqrt{2N_0\pi\sigma^2}} \tag{3}$$

where $\bar{\nu}$ is the mean molecular speed, N_0 is the Avogadro constant, and σ is the effective molecular collision diameter. This term K can then be adjusted to predict the effective transport coefficient (K_{eff}) of a single gas through a porous body. Using this approach should show that the presence of a porous, PMMA free outer layer gives rise to a moving boundary with a variable concentration of diffusant that depends upon the surface flux, gas transport coefficient, and thickness of the porous layer as stated by Lewis (1997).

5. Conclusion

Titanium components which have biocompatible properties have been produced via the MIM process. Details of the route which focuses on the debinding process have been discussed in terms of chemical reactions and also in terms of debinding kinetics. The final sintered products were evaluated against ASTM standard requirements. The tensile strength, elongation and oxygen levels within specification were achieved using the specially controlled debinding and sintering process to meet the requirements for Grade 2 titanium.

Therefore the titanium components fabricated exhibit potential for biomedical applications because the binder is completely removed before sintering. After sintering at high temperatures the parts are absolutely clean due to the protected atmosphere at high temperature. The fabrication route can be used for orthopaedic and dental products with complicated shapes.

Acknowledgements

The authors would like to thank Anglo Platinum and Yorkshire Forward for awarding grants to conduct the present research. The support of the Advanced Manufacturing Research Centre (AMRC) at the University of Sheffield is also gratefully acknowledged. Many thanks also go to Scott Bader and Egide (UK) for supplying Texicryl® PMMA Emulsion and mould tool equipment respectively.

References

Anwar, N.Y., 1996. Injection moulding of 316L stainless steel powder using novel binder system. PhD Thesis. University of Sheffield, Sheffield.
ASTM Standard F2885-11, 2011. Standard Specification for Metal Injection Molded Titanium–6Aluminum–4Vanadium Components for Surgical Implant Applications. American Society for Testing Materials (ASTM) International, West Conshohocken, PA.
ASTM Standard F67-06, 2006. ASTM F67-06, Standard Specification for Unalloyed Titanium for Surgical Implant Applications (UNS R50250, UNS R50400, UNS R50550, UNS R50700). American Society for Testing Materials (ASTM) International, West Conshohocken, PA.
ASTM Standard WK35394, 2011. New Specification for Standard Specification for Metal Injection Molded Commercially Pure Titanium Components for Surgical Implant Applications. American Society for Testing Materials (ASTM) International, West Conshohocken, PA.
Baril, E., Lefebvre, L.P., Thomas, Y., 2011. Interstitial elements in titanium powder metallurgy: sources and control. Powder Metall. 54 (3), 183–187.
Cao, M.Y., O'onnor, J.W., Chung, C.I., 1992. A new water soluble solid polymer solution binder for powder injection molding. In: Powder Injection Molding Symposium, San Francisco, CA, pp. 86–98.
Ebel, T., Blawert, C., Willumeit, R., Luthringer, B.J.C., Ferri, O.M., Feyerabend, F., 2011. Ti–6Al–4V–0.5B: a modified alloy for implants produced by injection molding. Adv. Eng. Mater. 13 (12), B440–B453.
Einhorn, R.A., Amoroso, N.J., Bogan, L.E., 1997. Novel feedstocks for powder injection molding. Ceram. Eng. Sci. Proc. 18 (2), 127–138.
Elias, H.G., 2003. An Introduction to Plastics, 2nd edition. Wiley-VCH GmbH, Weinhem (DE).
Elias, C.N., Lima, J.H.C., Valiev, R., Meyers, M.A., 2008. Biomedical applications of titanium and its alloys. JOM 60 (3), 46–49.
Eroglu, S., Bakan, H.I., 2005. Solvent debinding kinetics and sintered properties of injection moulded 316L stainless steel powder. Powder Metall. 48 (4), 329–332.
Ferri, O.M., Ebel, T., Bormann, R., 2009. High cycle fatigue behaviour of Ti–6Al–4V fabricated by metal injection moulding technology. Mater. Sci. Eng. A 504, 107–113.
Froes, F.H., 2005. Developments in Titanium P/M. Institute for Materials & Advanced Processes (IMAP), Moscow.
Froes, F.H., 2007. Advances in titanium metal injection molding. Powder Metall. Met. Ceram. 46 (5–6), 303–310.
Froes, F.H., German, R.M., 2000. Cost reductions prime Ti PIM growth. Met. Powder Rep. 55 (6), 12–21.
German, R.M., 1979. Gas flow physics in porous metals. Int. J. Powder Metall. 15 (1), 23–30.
German, R., 2009. Titanium powder injection moulding: a review of the current status of materials, processing, properties and applications. PIM Int. 3 (4), 21–37.
German, R.M., 2010. Status of metal injection molding of titanium. Int. J. Powder Metall. 46 (5), 11–17.
Hens, K.F., German, R.M., 1993. Advanced processing of advanced materials via powder injection molding. Adv. Powder Metall. Part. Mater. 5, 153–164.
Hsu, S.L., 1999. Poly(methyl methacrylate). In: Polymer Data Handbook. Oxford University Press, Oxford, pp. 655–657.
Jellinek, H.H.G., 1978. Degradation and depolymerization kinetics. In: Aspects of Degradation and Stabilization of Polymers. Elsevier, Lausanne/New York, pp. 1–37.
Joens, C.J., 2005. Laminar gas flows ensure 'clean sweep' in sintering. Met. Powder Rep. 60 (3), 52–55.
Kim, D.H., Lee, Y.W., Yoo, K.P., Lim, J.S., 2007. Separation of paraffin wax from ceramic injection molded part. Theor. Appl. Chem. Eng. 13 (1), 235–238.
Knudsen, M., 1909. Kinetic theory of gases. Ann. Phys. 28, 75.
Lewis, J.A., 1997. Binder removal from ceramics. Annu. Rev. Mater. Sci. 27, 147–173.
McCracken, M., 1999. Dental implant materials: commercially pure titanium and titanium alloys. J. Prosthodont. 8 (1), 40–43.
Omar, M.A., Ibrahim, R., Sidik, M.I., Mustapha, M., Mohamad, M., 2006. Rapid debinding of 316L stainless steel injection moulded component. J. Mater. Process. Technol. 140, 397–400.
Park, S.-J., Wu, Y., Heany, D.F., Zou, X., Gai, G., German, R.M., 2009. Rheological and thermal debinding behaviors in titanium powder injection molding. Metall. Mater. Trans. A 40, 215–222.
Petzoldt, F., Eifert, H., Hartwig, T., Veltl, G., 1995. Binder design and process control for high performance MIM-materials. Adv. Powder Metall. Part. Mater. 2, 6.3–6.13.
Shibo, G., Bohua, D., Xinbo, H., Xuanhui, Q., 2009. Powder injection molding of pure titanium. Rare Metals 28 (3), 261–265.
Shibo, G., Xuanhui, Q., Ting, Z., Bohua, D., 2006. Powder injection molding of Ti–6Al–4V alloy. J. Mater. Process. Technol. 173 (3), 310–314.
Sidambe, A.T., Figueroa, I.A., Hamilton, H.G.C., Todd, I., 2011a. Improved processing of titanium alloys by metal injection moulding. IOP Conf. Ser.: Mater. Sci. Eng., 26.
Sidambe, A.T., Figueroa, I.A., Hamilton, H., Todd, I., 2009. Sintering study of CP-Ti and Ti6V4Al metal injection moulding parts using Taguchi method. In: Proc. EuroPM 2009, EPMA, Mannheim, pp. 67–72.
Sidambe, A.T., Figueroa, I.A.F., Hamilton, H.G.C., Todd, I., 2011b. Taguchi optimization of MIM titanium sintering. Int. J. Powder Metall. 47 (6), 18–21.
Sidambe, A.T., Xu, W., Figueroa, I.A., Hamilton, H.G.C., Todd, I., 2008. Rapid debinding of a titanium component. In: Proc. EuroPM 2008, EPMA, Mannheim, pp. 275–280.
Song, J.H., Edirisinghe, M.J., Evans, J.R.G., Twizell, E.H.J., 1996. Modelling the effect of gas transport on the formation of defects during thermolysis of powder moldings. J. Mater. Res. 11, 830–840.
Tsai, D.S., 1991. Pressure build up and internal stresses during binder burnout: numerical analysis. AIChE J. 37, 547–554.
Wakao, N., Otani, S., Smith, J.M., 1965. Significance of pressure gradients in porous materials. Part I: diffusion and flow in fine capillaries. AIChE J. 11 (3), 435–439.
Yang, W.W., Yang, K.-Y., Wang, M.-C., Hon, M.-H., 2003. Solvent debinding mechanism for alumina injection molded compacts with water-soluble binders. Ceram. Int. 29 (7), 745–756.